

4.4

Self-Optimization of Optical Confinement and Lasing Action in Disordered Photonic Crystals

Alexey Yamilov

Missouri University of Science and Technology

Hui Cao

Yale University

CONTENTS

4.4.1	Introduction	395
4.4.2	Lasing in Random Media	396
4.4.2.1	Light Propagation in a Random Medium with Optical Gain	396
4.4.2.2	Random Lasing in Strongly Scattering Media	396
4.4.2.3	Absorption-Induced Confinement	397
4.4.2.4	From Random Medium to PhCs with Disorder	398
4.4.3	Confinement in Disordered PhCs	398
4.4.3.1	Disorder in Passive and Active PhC Structures	398
4.4.3.2	Optimal Degree of Disorder	399
4.4.4	Lasing in a Disordered PhC Slab	402
4.4.4.1	PhC Slab Laser: Design Considerations	402
4.4.4.2	Structure Parameters and the PBG	403
4.4.4.3	Spontaneous Optimization of In-Plane and Out-of-Plane Confinement... ..	404
4.4.5	Summary and Outlook	410
	Acknowledgments	410
	References	411

4.4.1 Introduction

Light scattering is usually regarded detrimental to optical confinement in conventional lasers. In contrast, in random lasers, the confinement is *caused* by disorder-induced scattering. In strongly scattering media, the lasing is defined by the high-quality modes of the passive system. Thus, by incorporating and optimizing a degree of order, one can dramatically reduce the threshold of a random laser to the values comparable to those of photonic crystal (PhC) lasers. Unlike the latter, where the optical cavity has to be carefully designed and impeccably fabricated, in disordered systems the modes originate from the structure imperfections unintentionally introduced during the fabrication process. Optical gain

selectively amplifies the high-quality modes of the passive system. Consequently, in PhC slab geometry, for example, the in-plane and out-of-plane leakage rates of the lasing modes can become automatically balanced in the presence of disorder. Such self-optimization of optical confinement makes disordered PhC structures a competitive platform for large-scale low-cost production of microlasers with fabrication requirements much less stringent than those of PhC lasers with designed cavities.

4.4.2 Lasing in Random Media

4.4.2.1 Light Propagation in a Random Medium with Optical Gain

Incorporating optical gain in a random medium adds a new dimension to studies of light transport. In 1968, Letokhov¹ considered the effect of light amplification on the photons propagating through a scattering medium. It was predicted that under some conditions the number of photons will increase exponentially similar to neutron reaction in an atomic bomb. One can understand this incoherent process, called random lasing, within the framework of one of the following two pictures.

Semiclassically, repeated scattering of a spontaneously emitted photon increases its path-length inside the medium. When the system dimensions are increased beyond a certain critical size, every photon, on an average, generates another photon before escaping radiatively. This random walk process can be described by models based on diffusion equations.^{1,2}

A modal picture provides another intuitive description of the process of random lasing.^{3,4} Spatially and spectrally overlapping leaky modes of the random medium compete for gain. Compensating the radiative losses for a large number of such modes by gain results in a narrowing of the gain spectrum. However, unlike conventional lasers the limiting linewidth is still broad, commonly, in a range of several nanometers, and the emission is not fully coherent.

4.4.2.2 Random Lasing in Strongly Scattering Media

For a little over a decade, there have been many studies on random lasers with *coherent feedback*.^{5,6} In a strongly scattering active medium, light may return to a coherence volume it has visited before, and self-interference provides resonant feedback for lasing. With sufficient gain, lasing oscillation might occur at discrete frequencies that are determined by the interference of scattered light.

Similar to the incoherent random lasing introduced above, both semiclassical and modal descriptions can provide valuable insights. Indeed, the photons with semiclassical loop trajectories would have to experience a self-interference effect.⁷ The resulting process of wavelength selectivity resembles that in a distributed feedback resonator.

Alternatively, a finite open system of scattering particles can be characterized by a set of quasistationary (leaky) optical modes. When optical gain is introduced to such a system and it is sufficient to compensate the loss in at least one mode, lasing occurs. Thus, the mode with the smallest loss or the highest quality tends to lase first, and its quality factor Q determines the lasing threshold.

Both semiclassical and the highest- Q modal pictures oversimplify the real problem—coherent random lasing and, in particular, its threshold, also depends on many factors.

A realistic estimate should involve a detailed account of the gain material properties and its spatial distribution, the variation of the local density of states in the system and its effect on light-matter interaction, the pumping scheme, the reabsorption of laser light, and so on. Therefore, finding the threshold of random laser theoretically is a complicated problem. Nevertheless, in the important case of a uniform gain and strong scattering, Q can become the determining factor. Studies of the high- Q modes supported by a random medium advanced our understanding of coherent random lasing.^{8–14}

4.4.2.3 Absorption-Induced Confinement

Coherent random lasing has been realized also in weakly scattering random media.¹⁵ Tight focusing of pump light was necessary to observe discrete lasing peaks, namely, the pump beam had to be focused to a region of size much smaller than the entire sample. Imaging of laser light on the sample surface revealed that the lasing modes were not extended over the entire random medium but instead were located inside the pumped region with an exponential tail outside it.¹⁶ As the quasimodes of a random system far from the onset of localization are usually extended states, the lasing modes were initially regarded as some types of anomalously localized states, either almost-localized states¹⁷ or prelocalized states.^{16,18} Although the anomalously localized states should be rare in the diffusive samples, the experiments always showed lasing modes that are spatially confined in the pumped region independent of where on the sample the pump beam is focused. Moreover, the lasing threshold did not fluctuate much as the pump spot was moved across the random medium.

In the study by Yamilov et al.,¹⁹ it was shown that the above contradiction to the theory of anomalously localized states originates from the assumption that lasing occurs in the quasimodes of the passive random medium. This assumption is not valid when absorption at the emission wavelength is significant outside the pumped volume. The reabsorption of emitted light suppresses the feedback from the unpumped part of the sample and effectively reduces the system size. The lasing modes are dramatically different from the quasimodes of the whole system without gain or absorption. Even if all the quasimodes of a passive diffusive system are extended across the entire sample, the experiments find that the lasing modes are still confined in the pumped volume with only an exponential tail outside it.

The reduction of the effective volume of the system V_{eff} as a result of absorption leads to a decrease of an important parameter that characterizes wave transport—Thouless number $\delta \equiv \delta v / \Delta v$, where δv and Δv are the average mode linewidth and spacing, respectively.²⁰ In a three-dimensional (3D) diffusive system, $\delta v \propto V_{\text{eff}}^{-2/3}$ and $\Delta v \propto V_{\text{eff}}^{-1}$, therefore, $\delta \propto V_{\text{eff}}^{1/3}$. The smaller the value of δ , the larger the fluctuation of the decay rates γ of the quasimodes.^{18,21} The variance of the decay rates¹⁸ $\sigma_{\gamma}^2 = \langle \gamma \rangle^2 / \delta$, where the average decay rate $\langle \gamma \rangle \sim D / V_{\text{eff}}^{2/3}$. Broadening of the decay rate distribution along with the decrease of the total number of quasimodes within V_{eff} should reduce the number of lasing modes (besides nonlinear mode competition via spatial hole burning, discussed in the study by Tureci et al.⁴), and, therefore, should be responsible for the observation of discrete lasing peaks in the tight focusing experiments. Despite its reduced value, the effective Thouless number is still much larger than unity owing to weak scattering. As a result, the lasing modes are the extended states within the effective volume. Because $\sigma_{\gamma} / \langle \gamma \rangle \ll 1$, the minimum decay rate is still close to $\langle \gamma \rangle$, leading to high threshold for lasing and its relatively small fluctuations.^{9,10,22}

4.4.2.4 From Random Medium to PhCs with Disorder

Random lasing has generated great excitement in the physics community.^{6,23} One of the most formidable problems on the way to practical applications is that lasing thresholds are too high because of incomplete confinement of light. To improve the confinement, one approach that has been used with some success is to maximize the scattering strength by using Mie resonances.^{24–26}

Another approach can be traced back to the pioneering work by John²⁷ who proposed to manipulate the effective momentum of light by introducing periodicity into the system. Ioffe-Regel criterion²⁸ for light localization in the presence of periodicity is replaced by $k_c \ell \sim 1$, where k_c is crystal momentum,²⁹ which is much smaller than the optical wavevector k near the band edge. This criterion compares the scattering mean free path ℓ to the effective wavelength $\propto k_c^{-1}$; it originates from the semiclassical description of light propagation. In the language of modes, the disorder creates high- Q defect states^{10,12,13,30} in the spectral tails that extend into the residual photonic band gap (PBG).³¹

4.4.3 Confinement in Disordered PhCs

4.4.3.1 Disorder in Passive and Active PhC Structures

In passive PhC devices, uncontrollable disorder introduced during the fabrication process has a detrimental effect^{32–35} as it contributes to optical losses and limits light propagation length even in the highly precise PhC slab waveguides.^{36–39} However, it is not immediately clear how the disorder would affect the performance of an *active* device such as, for example, a PhC slab laser.

Below we show that structural disorder in a PhC laser may not be as detrimental as it is in a passive PhC waveguide. In Section 4.4.3.2, we demonstrate theoretically that weakly disordered PhC structures can support high- Q optical cavities.^{10,12–14} Such cavities can be observed experimentally⁴⁰ and they can also facilitate lasing action.^{14,41–43}

A disordered PhC can be considered as a transition from a perfectly ordered structure to a completely random medium. In Section 4.4.3.2, we systematically investigate this disorder-induced transition in two-dimensional (2D) PhCs. We find that there exists an optimal degree of disorder that leads to the maximum (on average) confinement.¹⁰ In fact, we estimate that Q factor and mode volume of the quasimodes in such spontaneously formed microcavities is comparable to those in carefully designed defect modes in the perfectly ordered PhC. Of course, when making the generalizations one has to take into a consideration the particular type of disorder at hand, for example, correlated or uncorrelated disorder, particle size, and/or position disorder.⁴⁴ However, we believe that the main conclusion about the existence of the optimal degree of disorder remains generally valid. This can be understood with a simple argument. The localization length is shortest at the frequency in the middle of the PBG.²⁷ A disorder affects the PBG by making it spectrally broader and shallower—that is, increasing the localization length at the center of the gap.⁴⁵ However, because we are interested in creating an active device—a microlaser—we also have to take into consideration the probability of creating an optical cavity in any given configuration of disorder. When disorder is weak, the local fluctuations of the photonic band edge create so-called tail states³¹ that are the photonic equivalent of the Lifshitz states in the condensed matter systems.⁴⁶ The density of these states falls off rapidly, exponentially, for the frequencies deep

inside the PBG where the localization length is the shortest. This means that, at weak disorder, the tail states cannot take advantage of the maximum confinement. Therefore, the optimum degree of disorder appears as a balance between density of the tail states and their degree of confinement that show opposite trends with an increase of the disorder strength.¹⁰

The argument outlined above does not account for a possibility of purposefully creating a defect state in the middle of the PBG via certain PhC structure modifications. In Section 4.4.4.3, using a more realistic example of PhC slabs, we show that in the presence of disorder such a defect state may not be superior when other factors such as mode volume and vertical leakage are taken into account. Indeed, we show that because spatially uniform optical gain selectively amplifies the high- Q modes of the passive system, in PhC slabs the in-plane and out-of-plane leakage rates may be automatically balanced in the presence of disorder. The spontaneous optimization of in-plane and out-of-plane confinement of light in a PhC slab can lead to a reduction of the lasing threshold. Our experiments support these conclusions. Furthermore, concentration of the modes in the vicinity of the photonic band edge can enable an efficient extraction of gain. It also offers a possibility to fine-tune the lasing wavelength by, for example, changing the lattice constant (c.f. Section 4.4.4.3).

In the above, we approached the problem of minimization of the threshold of a random laser from the perspective of the *optimal degree of disorder* in a PhC. In fact, in our prior work we followed the opposite approach by searching for the *optimal degree of order* in random medium. This can be accomplished by studying the milestones in the transition from a random to periodic medium. First, we investigated experimentally and theoretically the effect of the zinc oxide (ZnO) scatterer size dispersion.²⁴ Also, we noted that PBG effects may become already noticeable in the randomly packed monodisperse spheres as a result of a short-range order—formation of the small ordered clusters.⁴⁷ This supposition was further confirmed in ZnO nano-structured dielectric films,⁴⁸ which exhibited a varying degree of short-range order.²⁵ ZnO structures with 2D long-range order^{14,42,49} and 3D long-range order^{43,50} were the third step in our systematic study of lasing in disordered media with variable degree of order. Small feature size, required in order to overlap the PBG with the gain spectrum of ZnO at near-ultraviolet frequency, resulted in relatively large degree of the residual fabrication disorder. Systems with 2D periodicity—PhC slab—gave us particularly many degrees of freedom to perform the combined experimental and theoretical studies of the effect of disorder. In the following, we will concentrate on the last step in our three-step study of the transition from random to ordered media—weakly disordered PhC slabs.

4.4.3.2 Optimal Degree of Disorder

In this section, we use the finite-difference time-domain method⁵¹ to find the highest-quality modes in open passive 2D random systems with various degrees of ordering. We consider a 2D $L \times L$ (up to $9\lambda \times 9\lambda$) PhC made of N ($\propto L^2$) cylinders with diameter $d = 98$ nm and refractive index $n_0 = 2.2$. The cylinders were arranged into a hexagonal lattice with nearest-neighbor distance $a = 140$ nm. In the absence of disorder, the infinite system with these parameters has full band gap in the range [361 nm, 426 nm] for transverse magnetic modes (electric field along the cylinder axis). The disorder in the system is introduced in two ways: by uniformly randomizing the refractive index n of different cylinders in the range $[n_0 - w_n(n_0 - 1), n_0 + w_n(n_0 - 1)]$ and diameter $[d(1 - w_d), d(1 + w_d)]$. Special care should be taken to avoid the uncontrollable disorder due to discretization of the grid. Disorder in the system is characterized with parameter $\delta\epsilon = \langle \int (\epsilon(\mathbf{r}) - \epsilon_0(\mathbf{r}))^2 d\mathbf{r} \rangle^{1/2} / (\int \epsilon_0^2(\mathbf{r}) d\mathbf{r})^{1/2}$, where $\epsilon_0(\mathbf{r})$ and $\epsilon(\mathbf{r})$ are the dielectric constant distributions in ordered and disordered samples,

respectively; $\langle \dots \rangle$ stands for the average over different disorder configurations. Here we study the systems with 11 different disorder strengths: 1 to 10 had w_n from 0.1 to 1.0 with the increment 0.1 and $w_d = 0$, the 11th has $w_n = 1.0$, and $w_d = 0.43$. This leads to variations of dielectric constant from weak $\delta\epsilon = 0.08$ to strong $\delta\epsilon = 0.95$ disorder. Later we will discuss the effect of this particular choice of the types of disorder. To mimic an open system, a buffer layer of air (150 nm thick) is kept around the sample, followed by uniaxial perfectly matched absorbing layers.⁵¹ To excite the system, we initially launched a short ~ 10 fs pulse at every grid point. The frequency ω_e of the pulse is chosen to lie at the center of the band gap (391 nm) of the ordered structure. In the frequency domain, the full-width at half-maximum of the excitation pulse is of the order of the band-gap width. Thus, the pulse excites all the modes within the stop band and near the band edges.

Right after the initial pulse, the competition between the modes⁵² with different lifetimes leads to the complicated evolution of total electric energy $\mathcal{E}(t) = 1/2 \int \epsilon(\mathbf{r}) \mathbf{E}^2(\mathbf{r}) d\mathbf{r}$. However, after a sufficient time only the mode with the longest lifetime (highest quality factor) survives. $\mathcal{E}(t)$ followed a monoexponential decay $Re[\exp 2i\omega_m(1 + i/2Q_m)t]$, from which we extract the frequency ω_m and quality factor Q_m of the longest-lived mode in this particular realization of disorder. At the same time, the spatial pattern, $\mathbf{E}(\mathbf{r})$, stabilizes and the mode profile can be seen. Generally, the time needed to reach the monoexponential decay regime varies from about 0.5 ps for the smallest system to 10 ps for the largest. Finally, the Q_m is averaged over 1000 ($N = 75$), or 100 ($N = 137, 188, 261, 368, 449, 608$) disorder realizations.

Figure 4.4.1 shows the dependence of $\langle Q_m \rangle$ normalized by N as a function of the disorderness $\delta\epsilon$; different curves correspond to different system sizes. This particular normalization makes it easy to see the deviation from diffusion-predicted¹ dependence $\langle Q_m \rangle \propto L^2 \propto N$. One can see that significantly different scalings at different $\delta\epsilon$ lead to a maximum of $\langle Q_m \rangle$ at the finite disorder strength.¹⁰

The understanding of this behavior comes from observing the frequencies ω_m of the highest-quality modes in Figure 4.4.2. For small $\delta\epsilon$ the frequencies are concentrated at lower (long wavelength) band edge, and they (as well as Q_m) are independent of the frequency ω_e of the excitation pulse. The reason for this is the way the disorder was introduced into the system. The long-wavelength modes are mostly concentrated in the dielectric cylinders, which are disordered by the refractive index fluctuations. At $w_n = 0.1$,

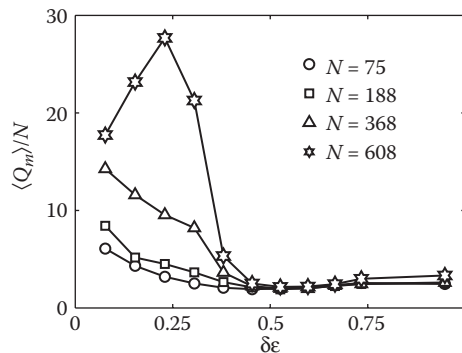


FIGURE 4.4.1

$\langle Q_m \rangle$ normalized by total number of scatterers N ($\propto L^2$) as a function of disorderness $\delta\epsilon$. The figure shows that with an increase of the system size a maximum of $\langle Q_m \rangle$ develops at a finite value of disorder strength $\delta\epsilon$. (Reprinted from A. Yamilov and H. Cao Phys. Rev. A **69**, 031803 (2004).)

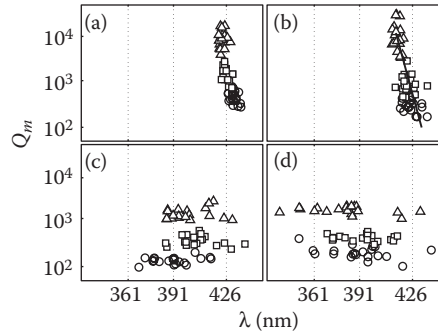


FIGURE 4.4.2

Q_m versus the corresponding mode wavelength for 20 realizations of disorder. Circles, squares, and triangles correspond to N equal to 75, 188, and 608, respectively. Four graphs correspond to different disorder parameters: (a) $w_n = 0.1$ ($\delta\epsilon \approx 0.08$), (b) $w_n = 0.2$ ($\delta\epsilon \approx 0.15$), (c) $w_n = 0.6$ ($\delta\epsilon \approx 0.45$), and (d) $w_n = 1.0$ and $w_d = 0.43$ ($\delta\epsilon \approx 0.95$). Concentration of the modes near one of the band edges of the photonic band gap (PBG) (361–426 nm) demonstrates the presence of the residual gap at weak disorder (a, b). Migration of the modes toward the PBG center in (b) with the increased system size causes the decrease of the localization length ξ . (Reprinted from A. Yamilov and H. Cao Phys. Rev. A **69**, 031803 (2004).)

ω_m fell in the immediate vicinity of the band edge (Figure 4.4.2a). Lasing from the band-edge modes is well studied in the case of ordered structures,^{63–65} with $Q_m \propto L^3$.¹¹ The latter indeed gives a good fit to our results.

At the increased disorder, $w_n = 0.2$ – 0.3 , the dependence of $\langle Q_m \rangle$ on the system size L became exponential, as expected for localized modes.⁶⁶ In the unit of wavelength the localization length ξ , obtained by fitting, decreased from 1.44λ to 1.27λ as w_n increased from 0.2 to 0.3. Figure 4.4.2b provides an insight into the physics behind the varying ξ . The quality factor can be estimated as $\langle Q_m \rangle \propto \exp[L/2\xi(\omega_m)]$, where $\xi(\omega_m)$ is the “typical” value of the localization length at the frequency ω_m . From Figure 4.4.2b one can see that even for the same disorder strength, the increase in system size leads to the advance of ω_m toward the band-gap center, where ξ is the smallest. This peculiar behavior should lead to superexponential dependence of $\langle Q_m \rangle$ on L even for fixed disorder strength. The frequency migration with the increase of the system size can be explained by the fact that in the small system it is unlikely to find the modes deep into the band gap owing to the low density of states there. An Urbach-like behavior can be expected.^{31,67} This is also qualitatively supported by Figure 4.4.2b where the exponential dependence is apparent. Assuming Urbach-like dependence of the density of states, the advancement of ω_m can be estimated from the condition that the total number of defect states (proportional to the number of cylinders N) times the probability of having a state located $\Delta\omega(N)$ away from the band edge, $\exp[-\alpha(\delta\epsilon) \cdot \Delta\omega(N)]$, is equal to one. Here, $\alpha(\delta\epsilon)$ is the exponential slope of the density of states that should decrease with the increase of the disorder $\delta\epsilon$. For small disorder $\alpha^{-1}(\delta\epsilon) \ll \Delta E_{\text{PBG}}$, where ΔE_{PBG} is the width of the PBG. Therefore, for weak disorder (or small system size) the band-edge-type modes have the highest Q . The crossover to the superexponential dependence of $\langle Q_m \rangle$ occurs when the Q of the localized states with the shortest localization length $\xi[\Delta\omega(N)]$ available for this size N exceeds that of the band-edge-type mode: $\exp[N^{1/2}a/\xi(\Delta\omega(N))] \sim N^{3/2}$. Stronger size dependence in the superexponential regime means that the $N^{3/2}$ band-edge-type dependence observed at smaller disorder would eventually switch to the superexponential dependence as N increases. However, the latter can be expected to saturate at larger size or disorder when ω_m reaches the band-gap center: $N \cdot \exp[-\alpha(\delta\epsilon)\Delta E_{\text{PBG}}/2] \sim 1$, where the

localization length is the smallest. Therefore, we expect the limiting scaling of $\langle Q_m \rangle$ to be exponential: $\langle Q_m \rangle \propto \exp[N^{1/2}a/2\xi(\Delta E_{\text{PBG}}/2)]$.

The sharp drop in $\langle Q_m \rangle$ at $\delta\epsilon \approx 0.34$ in Figure 4.4.1 is attributed to the removal of the residual band gap. This can be seen from the loss of the hexagonal symmetry of the observed mode profiles as well as the sensitivity of the modes to the excitation pulse position ω_e . In this regime, ω_m is not associated with the PBG, which does not exist anymore. However, to make a direct comparison with the ordered case, we kept the excitation pulse the same as before. The exact mechanism of the band-gap removal can depend on the disorder.^{10,31,33,34,68} In our particular case, we found a simple explanation for the behavior of $\langle Q_m \rangle$ in the way the disorder was introduced. Indeed, the fluctuating index of refraction leads to the fluctuation of the frequency of the Mie resonances of the particles. For box distribution of n , there exists a value of $w_n = 0.6$ when the Mie resonance of some defect cylinders falls into the gap. This value matches the value of disorder parameter $\delta\epsilon$, where the sharp decrease of $\langle Q_m \rangle$ is observed in Figure 4.4.1. Moreover, Figure 4.4.2c shows that at this crossover disorder, the modes avoid the region of strong single-particle scattering. This is the consequence of the sharp boundary in the distribution of n . It also indicates the presence of the residual band gap, where the ω_m are concentrated.

At $w_n \geq 0.7$ the PBG ceases to exist, and $\langle Q_m \rangle$ acquires the diffusion¹ scaling dependence: $\langle Q_m \rangle \propto L^2 \propto N$ (c.f. Figure 4.4.1). Deviations from this dependence can be seen in the same figure at the largest sizes studied, where $L > \xi_{\text{Anderson}} = 2.54\lambda$ is inferred and the states become localized again as a result of Anderson localization.⁶⁶ The exponential dependence of $\langle Q_m \rangle$ on L becomes especially pronounced at the largest disorder studied, where the transition from L^2 to exponential dependence comes at small system sizes. We want to point out that even at such strong disorder, the obtained modes had a collective nature, rather than the single particle's high-order resonances, which are concentrated at higher frequencies. Comparing the localization length of these states to that of band-gap nature we see a difference of a factor of two, which makes the latter preferable (c.f. Figure 4.4.1).

To summarize the results of this section, by varying the strength of disorder, we identified five different scaling regimes of the ensemble-averaged $\langle Q_m \rangle$ with the system size: (a) photonic band edge, L^3 , (b) transitional superexponential, (c) band-gap-related exponential, (d) diffusive, L^2 , and (e) disorder-induced exponential, due to Anderson localization, regimes. The difference in scaling behavior allows one to draw the following conclusions that provide an intuitive phenomenological picture of the disorder-induced transition: (i) For sufficiently wide band gaps, $\langle Q_m \rangle$ reaches a maximum at some finite strength of disorder; (ii) at this "optimal" degree of disorder, $\langle Q_m \rangle$ is determined by the localization length similar to that of single defect in the ordered structure, leading to a similar quality factor; (iii) with an increase of the system size the optimal disorder strength decreases; (iv) near this optimal disorderness, $\langle Q_m \rangle$ should scale superexponentially with the sample size, owing to the frequency migration of the highest-quality modes toward the band-gap center and the associated decrease of their localization lengths.

4.4.4 Lasing in a Disordered PhC Slab

4.4.4.1 PhC Slab Laser: Design Considerations

A PhC slab utilizes index guiding to confine light to the plane of the slab.^{69–71} In-plane confinement is realized either via a defect state located inside a PBG^{72–77} or a band-edge

state with vanishing group velocity.^{64,65,78–81} Over the past decade, tremendous progress has been made in design and fabrication of PhC slab lasers that operate at infrared or near-infrared frequencies.^{65,72–77,80,82} To realize a near-ultraviolet PhC slab laser, the feature size has to be reduced roughly by a factor of four^{42,49} compared to the infrared PhC. Fabrication of such fine structures inevitably generates random deviations from the perfectly ordered structures.

Design of a PhC slab laser involves determination of structural parameters to ensure spectral overlap between the PBG and the gain spectrum. In addition, lasing mode volume optimization is required owing to a planar geometry of the device. This is because light may escape from the PhC slab vertically through the top/bottom interfaces or laterally via the edge of the periodic pattern into air or unpatterned part of the slab. The vertical leakage rate is characterized by the out-of-plane energy loss per optical cycle Q_{\perp}^{-1} , and the lateral by Q_{\parallel}^{-1} . A defect state spatially localized in the vicinity of an intentionally introduced structural defect typically has large leakage in the vertical direction, that is, $Q_{\perp}^{-1} \gg Q_{\parallel}^{-1}$. For a band-edge state, the lateral leakage usually dominates over the vertical one, $Q_{\parallel}^{-1} \gg Q_{\perp}^{-1}$. The total loss is described by $Q_{\text{tot}}^{-1} = Q_{\perp}^{-1} + Q_{\parallel}^{-1}$. Low lasing threshold demands maximization of Q_{tot} , which is hindered by Q_{\perp} for a defect state and Q_{\parallel} for a band-edge state. Several designs aim at optimization of PhC slab lasers by balancing Q_{\perp} and Q_{\parallel} via “gentle localization,”⁷⁵ for example, phase-slip,^{74,83} double-heterostructure.⁷⁷

Using disorder-induced defect modes allows one to relax stringent requirements for the residual fabrication disorder. Furthermore, the last step in optimization—mode-volume optimization—can be accomplished spontaneously by the disorder. Therefore, disorder optimization appears as an additional design parameter that can maximize Q_{tot} without the need to repeat previous optimization steps. Below we illustrate the above approach with the combined experimental and theoretical study of ZnO-based disordered PhC slab near-ultraviolet lasers.

4.4.4.2 Structure Parameters and the PBG

A typical PhC slab made of III-V semiconductors is a free-standing membrane structure, whose substrate is selectively etched away so that there is air both above and below the photonic layer. Although such a structure can achieve wider in-plane PBG and better light confinement in the vertical direction, it poorly dissipates heat and it is usually mechanically fragile. Also it is difficult to make a large area fabrication and cannot be applied to on-chip fabrication easily. In our case, the ZnO photonic layer is fabricated on a lattice-matched sapphire substrate. Such a structure is much more robust and easier for large-scale on-chip applications. On the other hand, owing to the lower refractive index contrast between the photonic layer and the substrate, light confinement in the vertical direction is worse than that in the free-standing layer, and the in-plane PBG is also narrower. In this case, the defects introduced during fabrication are supposed to be even more detrimental to PhC slab lasers.

To simulate a PhC slab on a dielectric substrate, we modified⁴² the super-cell technique⁷⁰ within the plane-wave expansion method for the photonic band-structure calculation.⁸⁴ A substrate with high refractive index is expected to significantly mix the polarization of eigenmodes of the PhC slab. However, our calculations demonstrate that although the substrate indeed induces asymmetry of wavefunctions, they still remain strongly transverse magnetic- or transverse electric-polarized for low-order bands.⁴² A high filling fraction air-hole-in-ZnO-matrix geometry can possess a complete PBG for transverse electric bands;

meanwhile, ZnO film with c -axis along the growth direction emits mainly into transverse electric-polarized modes. This enabled us to build a near-ultraviolet PhC slab laser.⁴² In the photonic band-structure calculation, we find the optimum set of parameters for maximum PBG: $R/a \approx 0.24$ and $t/a \approx 1.45$, where R is the hole radius, a is the lattice constant, and t is the slab thickness. These parameters are significantly different from the typical parameters for infrared PhC slabs. This is because of several factors: (i) the presence of the sapphire substrate breaks vertical symmetry of the PhC slab; (ii) the refractive index contrast of ZnO/sapphire is lower than that of InP/air commonly used in an infrared PhC slab; (iii) to preserve guiding in the photonic layer, the filling fraction and the thickness of the ZnO PhC slab need to be significantly increased.

Overlapping the PBG with the emission spectrum of ZnO requires precise control of the designed pattern with $a \approx 123$ nm, $t \approx 180$ nm, and $R \approx 30$ nm. This has been achieved with the focused ion beam (FIB) etching technique.⁴² The maximum relative width of PBG that can be achieved via optimization is 5%. This is significantly smaller than what is used in the free-standing membrane in air^{65,72,76} or in the case of low refractive index substrate.^{71,85} A narrow gap makes it difficult to align an intentionally introduced defect mode inside a PBG. However, there should always be some defect modes with frequencies inside PBGs formed as a result of the disorder introduced unintentionally during the fabrication process.

4.4.4.3 Spontaneous Optimization of In-Plane and Out-of-Plane Confinement

Using the parameters obtained in the previous section we realized the first near-ultraviolet PhC slab laser.⁴² ZnO films were grown on sapphire substrates by plasma-enhanced metalorganic chemical vapor deposition.⁴⁸ Hexagonal arrays of cylindrical air voids were patterned in the ZnO films by the FIB etching technique. Post-thermal annealing was used to remove the FIB damage. Single-mode lasing at room temperature was realized with optical pumping. The scanning electron micrograph (SEM) of a ZnO PhC slab is shown in Figure 4.4.3. Despite the long-range periodicity, Figure 4.4.3 reveals the deviation of the fabricated pattern from the ideal honeycomb structure. Such “crescent” deviation³⁵ caused optical scattering on the length scale of a few lattice constants. It was expected to enhance radiative leakage of a PhC slab laser based on either defect state¹² or band-edge mode. Moreover, the propagation loss in a passive PhC slab caused by random^{36,38,86} scattering was predicted to increase dramatically near a photonic band edge,³⁷ where the band-edge-type PhC slab laser operates. Despite these pessimistic expectations based on passive systems, we show that the performance of a PhC slab laser may be less susceptible to the detrimental effects of structural disorder. This is because optical gain predominantly amplifies the mode with the highest quality factor Q_{tot} . For the highest- Q_{tot} mode, the vertical and lateral leakage rates may be automatically balanced in the presence of disorder. This implies that an appropriate amount of structural disorder could lead to spontaneous optimization of in-plane and out-of-plane confinement of light in a PhC slab.

To investigate how the disorder affects the rates of vertical and lateral leakages of light from a PhC slab, we consider a system schematically depicted in Figure 4.4.4a. A dielectric slab of thickness 180 nm and refractive index $n = 2.35$ is sandwiched between air and substrate ($n_{\text{sub}} = 1.78$). Within the slab, N infinitely long grooves run parallel to the y -axis. The width of a groove is 22 nm; the lattice constant of the disorderless structure is 100 nm. We consider light propagating in the x - z plane, with the electric field along the y -axis. Such a system is 2D, which allows numerical simulation of large statistical ensembles of random systems. Despite the simplification, the system in Figure 4.4.4a retains the property essential for our study of the PhC slab laser—the possibility of vertical (along z -axis) and lateral

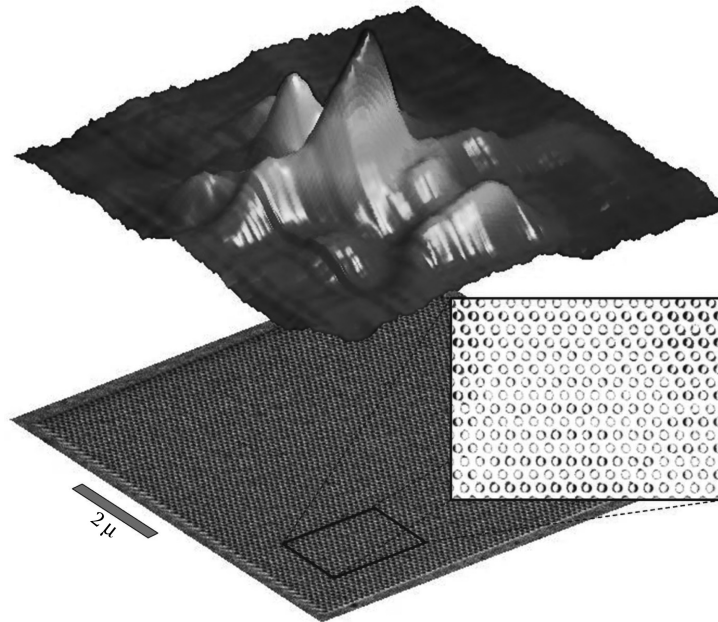


FIGURE 4.4.3

(See color insert.) Top-view scanning electron micrograph (SEM) of a ZnO photonic crystal (PhC) slab. Difference between the digitized SEM of a real sample and the perfect honeycomb lattice (blow-out box) reveals the structural disorder. Superimposed is the measured intensity distribution of the lasing mode in a ZnO PhC slab with $a = 115$ nm and $R = 0.25a$. The pattern measures 8×8 μm .

(along x -axis) radiative escape. Using the finite-difference time-domain method, we find the mode of the passive system that has the highest Q_{tot} .¹⁰ A Gaussian pulse was launched at all spatial points in the slab and the energy was allowed to leak out radiatively. Simulation area is terminated by a uniaxially perfectly matched absorbing layer that absorbs all outgoing waves. The pulse excites all modes within a 30 nm wavelength range around 400 nm. After the initial multimode decay the field distribution is stabilized and the longest-lived mode can be seen. This is further confirmed by observing a monoexponential decay of the total energy^{10,81,87} stored in the system that allows determination of Q_{tot} . By integrating Poynting vector over the corresponding interfaces,^{82,87} we obtained the outgoing flux in the vertical and horizontal directions, and Q_{\perp} and Q_{\parallel} . In our simulation, $Q_{\text{tot}}^{-1} = Q_{\perp}^{-1} + Q_{\parallel}^{-1}$ relation was satisfied numerically to within 2%.

Fourier transform of the spatial profile of the electric field at the interface between the slab and substrate gives the mode's distribution in k_{\parallel} (in-plane component of the wavevector) space. In a perfectly periodic structure, the band-edge mode has the highest Q_{tot} . It is spatially extended in x (c.f. Figure 4.4.4b), and thus has a narrow distribution in k_{\parallel} (c.f. thick dashed curve in Figure 4.4.5a). Next, we intentionally create a defect by increasing the spacing between two neighboring grooves at the center of the pattern to 150 nm. The highest- Q_{tot} mode is localized around this artificial defect with a localization length of 140 nm. Strong localization in x (c.f. Figure 4.4.4c) results in a broad distribution in k_{\parallel} (c.f. thin dashed curve in Figure 4.4.5a), with the maximum lying closer to the edge of substrate light-cone (c.f. dash-dotted vertical line in Figure 4.4.5a). Its Q_{tot} is limited by Q_{\perp} , which is about three times smaller than the corresponding Q_{\parallel} in a system of $N = 24$. In contrast, the

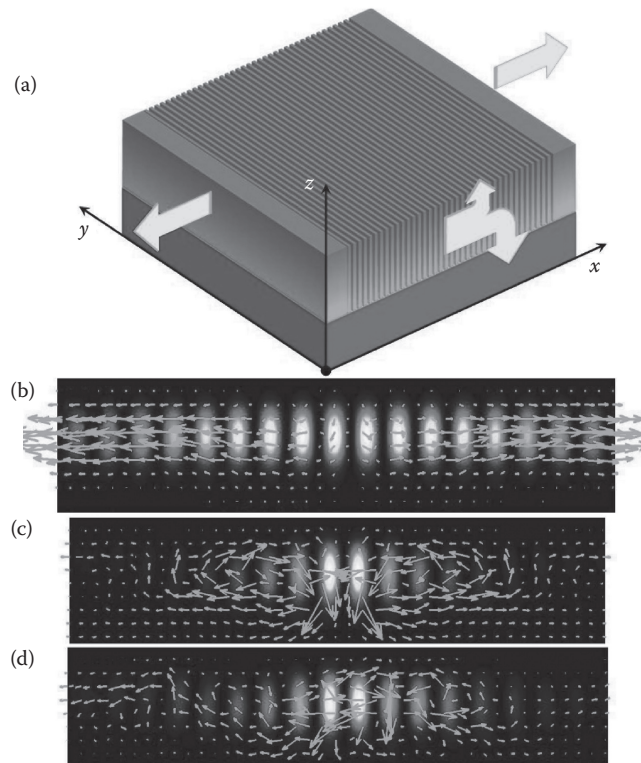


FIGURE 4.4.4

(See color insert.) (a) Simplified model of a photonic crystal slab used in numerical simulations. Infinitely long grooves run parallel to the y -axis. Disorder only affects x position of the grooves. Although such a system can be modeled in two dimensions—in the xz -plane—it already incorporates the possibilities of vertical and horizontal leakage. Intensity of the mode with the highest Q factor in (a) an ordered system (band-edge mode), (b) an ordered structure with a localized defect, and (c) a disordered structure with a localized defect. Arrows represent the amplitude and direction of the local Poynting vector. The radiative losses are dominated by in-plane leakage in (b) and by out-of-plane leakage in (c), whereas both loss mechanisms are comparable in the disordered system (d).

band-edge mode is concentrated well beyond the light-cone in k_{\parallel} -space; thus its Q_{\perp} is much higher. However, its spatial extension makes the lateral leakage larger; hence its Q_{tot} is limited by Q_{\parallel} .

To simulate the position disorder of air cylinders in real structure (c.f. Figure 4.4.3), random variation of groove position x_n is introduced. We choose Δx_n randomly from a uniform distribution with the standard deviation $\delta x = 5, 10, \text{ and } 15 \text{ nm}$, where δx characterizes the “strength” of disorder. As the disorder is introduced, the highest- Q_{tot} state differs from realization to realization, and the correspondent Q_{\parallel}, Q_{\perp} as well as the frequency vary. We study statistical distributions of these parameters and their dependences on disorder strength δx and system size N .

In small systems ($N = 12$ and 24) with an artificial defect and weak disorder ($\delta x = 5 \text{ nm}$), the highest- Q_{tot} modes always concentrate around the defect at the center of the pattern. These modes become more spatially extended than those without disorder (c.f. Figure 4.4.4d). Therefore, their k_{\parallel} distribution is narrowed and k_{\parallel} component within the light-cone is significantly reduced (c.f. Figure 4.4.5a). This reduction leads to a decrease in the

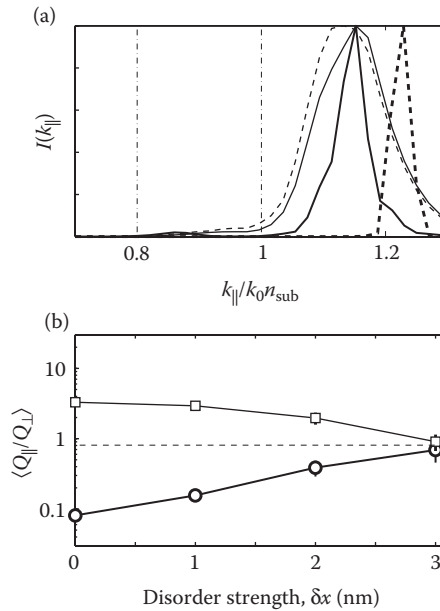


FIGURE 4.4.5

(a) The k_{\parallel} distributions of the highest- Q_{tot} modes at one pixel beneath the slab/substrate interface. Thin/thick dashed curve represents the mode found in the disorderless system ($N = 24$) with/without an artificial defect. The corresponding solid curves are representative examples of the highest- Q_{tot} modes in these systems with position disorder ($\delta x = 10$ nm). The vertical line marks the substrate light-cone boundary. The inset is a schematic sketch of the simulated structure. (b) Squares/circles represent $\langle Q_{\parallel}/Q_{\perp} \rangle$, averaged over 300 random realizations of $N = 24$ system with/without the artificial defect, versus disorder strength δx . (Reprinted from A. Yamilov et al., Phys. Rev. Lett. **96**, 083905 (2006).)

vertical leakage and, thus, an increase in Q_{\perp} . Meanwhile, Q_{\parallel} starts increasing as the mode gets less localized in real space. The ensemble-averaged $\langle Q_{\parallel}/Q_{\perp} \rangle$, shown in Figure 4.4.5b, decreases monotonously to unity with increase in disorder strength. Therefore, *disorder removes the imbalance between vertical and lateral leakages* of a single defect state, making $\langle Q_{\parallel} \rangle \sim \langle Q_{\perp} \rangle$. As a result, the ensemble-averaged quality factor $\langle Q_{\text{tot}} \rangle$ is slightly higher than that without disorder. In a larger system or with stronger disorder, the highest- Q_{tot} mode is no longer pinned at the artificial defect. Instead, it can explore the entire pattern to find the optimum configuration for the best vertical and lateral confinement. This leads to a further increase in $\langle Q_{\text{tot}} \rangle$.

With the introduction of disorder, the band-edge mode becomes less extended. As its “tail” moves away from the boundaries of the pattern, the lateral leakage decreases, and thus Q_{\parallel} increases. Meanwhile, the distribution in k_{\parallel} space is broadened and shifted closer to the light-cone edge (c.f. Figure 4.4.5a). The increase in vertical leakage results in a decrease in Q_{\perp} . The ensemble-averaged $\langle Q_{\parallel}/Q_{\perp} \rangle$, shown in Figure 4.4.5b, rises continuously to unity with increasing disorder strength. Again, disorder balances the vertical and lateral leakages of the band-edge mode, as it does to the defect state. However, for a band-edge mode the increase in $\langle Q_{\parallel} \rangle$ is not as large as the decrease in $\langle Q_{\perp} \rangle$; thus $\langle Q_{\text{tot}} \rangle$ is slightly lower than that without disorder. Nevertheless, as the pattern size N increases, the total leakage rate decreases monotonically: $\langle Q_{\text{tot}}^{-1} \rangle \propto N^{-\alpha}$ (c.f. Figure 4.4.6a). The exponent α decreases from 2.3 at $\delta x = 5$ nm to 1.9 at $\delta x = 15$ nm. Even with the largest disorder

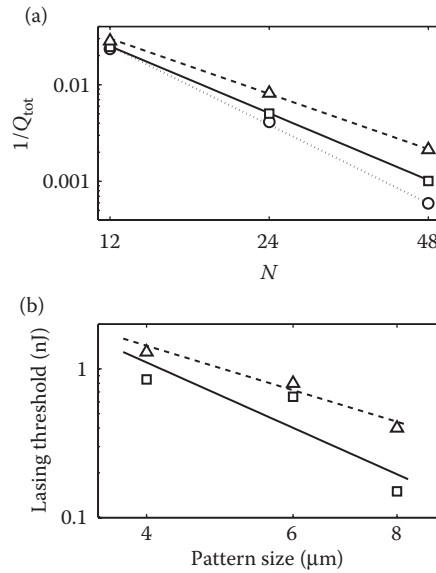


FIGURE 4.4.6

(a) $\langle 1/Q_{\text{tot}} \rangle$ for the highest- Q_{tot} modes found numerically in a photonic crystal slab depicted in the inset of Figure 4.4.3a. The average is taken over an ensemble of 300 random realizations. The squares and triangles represent the results for $\delta x = 5$ and 15 nm, respectively. Circles correspond to the disorderless system. Dotted, solid, and dashed lines are $N^{-\alpha}$ fits with $\alpha = 2.7$, 2.3, and 1.9, respectively. (b) Ensemble-averaged incident pump pulse energy at the lasing threshold, measured in the samples of $a = 115$ nm (squares) and $a = 118$ nm (triangles), versus the pattern size. The data are fitted with the power law dependence as in (a) with $\alpha = 2.5$ (solid line) and $\alpha = 1.7$ (dashed line). (Reprinted from A. Yamilov et al., Phys. Rev. Lett. **96**, 083905 (2006).)

we simulated ($\delta x = 15$ nm), no saturation of $\langle Q_{\text{tot}}^{-1} \rangle$ with N is observed up to $N = 48$. This behavior differs fundamentally from that of a PhC waveguide, where optical loss increases exponentially with its length. In contrast, a disordered PhC slab laser *benefits* from an increase in the pattern size, simply because a larger system provides a bigger pool of modes from which the highest- Q_{tot} mode can be selected. This effect should be more pronounced in PhC slab microlasers with 2D periodicity (c.f. Figure 4.4.3) as a result of the larger phase space compared to the numerically simulated systems with one-dimensional periodicity.

Experimentally, we fabricated ZnO PhC slabs of dimensions 4×4 , 6×6 , and 8×8 μm (c.f. Figure 4.4.3). As the complete PBG in a ZnO PhC slab without “undercut” was quite narrow,⁴⁹ it was technically challenging to overlap the PBG with the ZnO gain spectrum. By adjusting the magnification of the FIB system, we were able to change the lattice constant a in fine steps of 3 nm over a wide range 100–160 nm. The ratio of the air hole radius R to the lattice constant a was also varied from 0.20 to 0.30. In this way, we could tune the PBG continuously through the ZnO gain spectrum. We also introduced an artificial defect by missing an air hole. Structural analysis as in Figure 4.4.3 gives the average displacement of a hole $\delta r \approx 0.22R$.

A ZnO PhC slab was optically pumped by the third harmonics of a pulsed Nd:YAG laser ($\lambda = 355$ nm, 10 Hz repetition rate, 20 ps pulse width) at room temperature.⁴² In 8×8 μm patterns without intentionally introduced structural defect, the ensemble-averaged lasing threshold exhibited a pronounced minimum at $a = 113$ – 124 nm and $R = 0.25a$

(c.f. Figure 4.4.7a). To understand this phenomenon, we calculated the photonic bands in a ZnO PhC slab using the computational technique described by Yamilov et al.⁴⁹ The frequency dependence of the ZnO refractive index was taken into account. In Figure 4.4.7b, the wavelength of the dielectric band edge λ_d for the fundamental PBG of transverse electric modes⁴² is plotted against the lattice constant a . The structural parameters were extracted from the SEM of our samples. The ZnO slab thickness $t = 180$ nm, and $R/a = 0.245$. By comparing the lasing wavelength to λ_d in Figure 4.4.7b, we confirmed that the lasing modes were located in the vicinity of the dielectric band edge. This can be explained by two factors: (i) the electric field of the modes near the dielectric band edge is concentrated inside ZnO, and thus experience more gain; (ii) the vanishing group velocity at the band edge enhances light amplification.^{64,78,81} The dip in the measured lasing threshold (c.f. Figure 4.4.7a) is attributed to spectral overlap of the dielectric band edge with the ZnO gain spectrum. In Figure 4.4.6b, the measured lasing threshold decreases monotonously with the pattern size for $a = 115$ and 118 nm. These data agree qualitatively with the numerical simulation results shown in Figure 4.4.3a. In all patterns with intentionally missed air holes, the lasing modes were not pinned at the location of the missing hole owing to the existence of better-confined modes away from the defect. This observation is in line with our numerical simulation of large patterns with a single artificial defect.

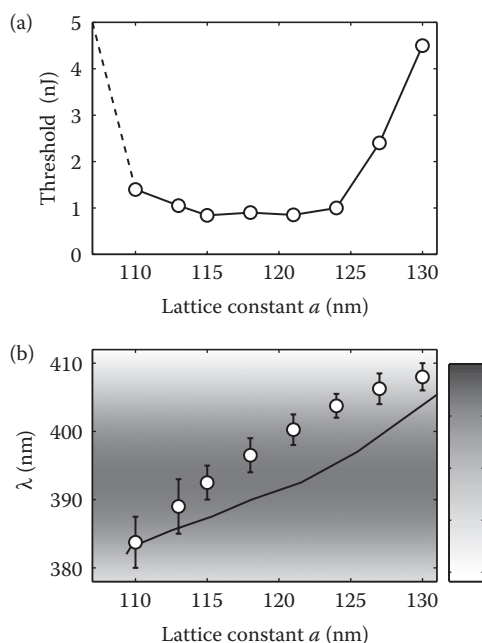


FIGURE 4.4.7

(a) Experimentally measured incident pump pulse energy at the lasing threshold (averaged over 5–10 samples) as a function of lattice constant a . (b) The circles are the measured mean wavelength of lasing modes; the error bar depicts the range of lasing wavelengths. The solid curve represents the wavelength of the calculated dielectric band edge λ_d in a ZnO photonic crystal slab as a function of a . The shade of the background qualitatively describes the position and width of the ZnO gain spectrum. This demonstrates the possibility of tuning lasing frequency of the devices by adjusting its lattice constant. (Reprinted from A. Yamilov et al., *Phys. Rev. Lett.* **96**, 083905 (2006).)

4.4.5 Summary and Outlook

In summary, with the combined theoretical and experimental studies, we find that the structural disorder may lead to self-optimization of optical confinement in a PhC slab and formation of high- Q_{tot} modes that serve as the lasing modes. In a sufficiently large PhC slab with uncorrelated disorder, a microcavity with balanced Q_{\perp} and Q_{\parallel} can be formed spontaneously without any carefully designed structural defects. In our near-ultraviolet PhC slab laser, random scattering by structural disorder leads to in-plane localization of band-edge modes. The underlying physical mechanism is similar to that of light localization in random media. The reduction of density of states near the photonic band edge enhances the localization effect. The most confined modes are selectively amplified in the presence of optical gain owing to long photon lifetime. We also demonstrate that despite the disorder, the band-edge effect allows one to fine-tune the lasing wavelength from 383 to 407 nm with sample-to-sample fluctuation of about 5 nm in the disordered ZnO PhC slab laser.

Our study questions the conventional wisdom that structural disorder always *degrades* the functionality of optical devices. Instead, we suggest that one needs to determine the type of disorder and understand its effects. Using lasing in disordered PhC slabs as an example, we demonstrate that a disorder can actually *enhance* the functionality of certain applications. Therefore, the strength and properties of the disorder emerge as additional tuning parameters. Although the above conclusions have been drawn on the basis of our analyses of PhC slabs that exhibit 2D periodicity, we believe they are quite general. There have been several reports of lasing in disordered 3D PhCs,^{56,88} however, much more work needs to be done to fully understand the intricacies of the interplay between order and disorder in these systems.

Another aspect of our study—the interplay between light transport in disordered systems and amplification—presents a fundamental interest. Indeed, the coherent amplification/absorption nontrivially affects the interferences of multiply-scattered waves and, thus, can promote/suppress localization phenomena. This observation has motivated us to begin systematically exploring an intriguing possibility of localization by gain—an enhancement of the mesoscopic phenomena with an increase of the amplification strength.⁸⁹

In this work, we discussed the disorder-induced transition from a perfectly periodic structure to a completely random medium. Although lasers based on disordered media can exhibit a variety of interesting behaviors, one of their limitations to device applications is the lack of control and reproducibility of the lasing modes. Recently, deterministic aperiodic structures attracted a great deal of attention. They also lie in between the periodic and random structures, ranging from quasicrystals to pseudorandom structures and, hence, spanning the entire spectrum in a hierarchy of complexity. Because of their structural distinction and unusual physical properties, the aperiodic systems have even been called the third form of solid matter.⁹⁰ The possibility of engineering lasing modes in deterministic structures with aperiodic ordering appears to be extremely promising.⁹¹

Acknowledgments

This work was supported by National Science Foundation under Grant Nos. DMR-0093949, ECS-0244457, DMR-0704981, ECCS-0823345, and DMR-0808937.

References

1. V. S. Letokhov, *Sov. Phys. JETP* **26**, 835 (1968).
2. N. M. Lawandy, R. M. Balachandran, A. S. L. Gomes, and E. Sauvain, *Nature* **368**, 436 (1994); D. S. Wiersma and A. Lagendijk, *Phys. Rev. E* **54**, 4256 (1996); R. Frank, A. Lubatsch, and J. Kroha, *J. Opt. A* **11**, 114012 (2009).
3. L. Florescu and S. John, *Phys. Rev. Lett.* **93**, 013602 (2004); G. Hackenbroich, *J. Phys. A* **38**, 10537 (2005); L. Angelani, C. Conti, L. Prignano, G. Ruocco, and F. Zamponi, *Phys. Rev. B* **76**, 064202 (2007); J. Andreasen et al. *Adv. Opt. Photon.* **3**, 88 (2011).
4. H. E. Tureci, L. Ge, S. Rotter, and A. D. Stone, *Science* **320**, 643 (2008).
5. H. Cao, *J. Phys. A* **38**, 10497 (2005).
6. H. Cao, *Opt. Photon. News* **16**, **24** (2005); D. S. Wiersma, *Nat. Phys.* **4**, 359 (2008).
7. H. Cao, Y. Zhao, S. T. Ho, E. W. Seelig, Q. H. Wang, and R. P. H. Chang, *Phys. Rev. Lett.* **82**, 2278 (1999).
8. X. Jiang and C. M. Soukoulis, *Phys. Rev. E* **65**, 025601 (2002); P. Sebbah and C. Vanneste, *Phys. Rev. B* **66**, 144202 (2002).
9. M. Patra, *Phys. Rev. E* **67**, 016603 (2003).
10. A. Yamilov and H. Cao, *Phys. Rev. A* **69**, 031803 (2004).
11. A. L. Burin, H. Cao, G. C. Schatz, and M. A. Ratner, *J. Opt. Soc. Am. B* **21**, 121 (2004).
12. A. Rodriguez, M. Ibanescu, J. D. Joannopoulos, S. G. Johnson, *Opt. Lett.* **30**, 3192 (2005).
13. M. A. Kaliteevski, D. M. Beggs, S. Brand, R. A. Abram, and V. V. Nikolaev, *Phys. Rev. E* **73**, 056616 (2006).
14. A. Yamilov, X. Wu, X. Liu, R. P. H. Chang, and H. Cao, *Phys. Rev. Lett.* **96**, 083905 (2006).
15. S. V. Frolov, Z. V. Vardeny, and K. Yoshino, *Phys. Rev. B* **59**, R5284 (1999); Y. Ling, H. Cao, A. L. Burin, M. A. Ratner, X. Liu, and R. P. H. Chang, *Phys. Rev. A* **64**, 063808 (2001).
16. H. Cao, Y. Ling, J. Y. Xu, and A. L. Burin, *Phys. Rev. E* **66**, R025601 (2002).
17. V. M. Apalkov, M. E. Raikh, and B. Shapiro, *Phys. Rev. Lett.* **89**, 016802 (2002); R. C. Polson, M. E. Raikh, and Z. V. Vardeny, *Physica E* **13**, 1240 (2002).
18. A. Mirlin, *Phys. Rep.* **326**, 259 (2000).
19. A. Yamilov, X. Wu, H. Cao, and A. L. Burin, *Opt. Lett.* **30**, 2430 (2005).
20. D. J. Thouless, *Phys. Rev. Lett.* **39**, 1167 (1977).
21. A. A. Chabanov, Z. Q. Zhang, and A. Z. Genack, *Phys. Rev. Lett.* **90**, 203903 (2003).
22. A. L. Burin, H. Cao, and M. A. Ratner, *Physica B* **338**, 212 (2003).
23. M. A. Noginov, *Solid-State Random Lasers* (Springer Science + Business Media, Inc., New York, 2005).
24. X. H. Wu, A. Yamilov, H. Noh, H. Cao, E. W. Seelig, and R. P. H. Chang, *J. Opt. Soc. Am. B* **21**, 159 (2004).
25. X. Liu, A. Yamilov, X. Wu, J. Zheng, H. Cao, and R.P.H. Chang, *Chem. Mater.* **16**, 5414 (2004).
26. S. Gottardo, R. Sapienza, P. D. Garcia, A. Blanco, D. S. Wiersma, and C. Lopez, *Nat. Photonics* **2**, 429 (2008).
27. S. John, *Phys. Rev. Lett.* **58**, 2486 (1987).
28. A. F. Ioffe and A. R. Regel, *Prog. Semicond.* **4**, 237 (1960).
29. S. John, *Phys. Rev. Lett.* **53**, 2169 (1984).
30. J. Topolancik, B. Ilic, and F. Vollmer, *Phys. Rev. Lett.* **99**, 253901 (2007).
31. J. M. Frigerio, J. Rivory, and P. Sheng, *Opt. Commun.* **98**, 231 (1993).
32. S. Fan, P. R. Villeneuve, and J. D. Joannopoulos, *J. Appl. Phys.* **78**, 1415 (1995); V. N. Astratov, A. M. Adawi, S. Fricker, M. S. Skolnick, D. M. Whittaker, and P. N. Pusey, *Phys. Rev. B* **66**, 165215 (2002).
33. M. M. Sigalas, C. M. Soukoulis, C. T. Chan, R. Biswas, and K. M. Ho, *Phys. Rev. B* **59**, 12767 (1999).
34. Z. Y. Li and Z. Q. Zhang, *Phys. Rev. B* **62**, 1516 (2000).
35. A. F. Koenderink, A. Lagendijk, and W. L. Vos, *Phys. Rev. B* **72**, 153102 (2005).

36. M. Skorobogatiy, G. Begin, and A. Talneau, *Opt. Express* **13**, 2487 (2005).
37. S. Hughes, L. Ramunno, J. F. Young, and J. E. Sipe, *Phys. Rev. Lett.* **94**, 033903 (2005).
38. D. Gerace and L. C. Andreani, *Opt. Express* **13**, 4939 (2005).
39. R. Ferrini, D. Leuenberger, R. Houdré, H. Benisty, M. Kamp, and A. Forchel, *Opt. Lett.* **31**, 1426 (2006); L. O'Faolain, T. P. White, D. O'Brien, X. D. Yuan, M. D. Settle, and T. F. Krauss, *Opt. Express* **15**, 13129 (2007); R. J. P. Engelen, D. Mori, T. Baba, and L. Kuipers, *Phys. Rev. Lett.* **101**, 103901 (2008).
40. J. Topolancik, B. Ilic, and F. Vollmer, *Appl. Phys. Lett.* **91**, 201102 (2007).
41. M. N. Shkunov, M. C. DeLong, M. E. Raikh, Z. V. Vardeny, A. A. Zakhidov, and R. H. Baughman, *Synth. Met.* **116**, 485 (2001); V. Milner and A. Z. Genack, *Phys. Rev. Lett.* **94**, 073901 (2005).
42. X. Wu, A. Yamilov, X. Liu, S. Li, V. P. Dravid, R. P. H. Chang, and H. Cao, *Appl. Phys. Lett.* **85**, 3657 (2004).
43. M. Scharrer, H. Noh, X. Wu, M. A. Anderson, A. Yamilov, H. Cao, and R. P. H. Chang, *J. Opt.* **12**, 024007 (2010).
44. S. F. Liew and H. Cao, *J. Opt.* **12**, 024011 (2010).
45. C. M. Soukoulis, ed., *Photonic Crystals and Light Localization in the 21st Century* (Kluwer Academic Publishers, Dordrecht, The Netherlands, 2001).
46. I. M. Lifshitz, *Sov. Phys. Usp.* **7**, 549 (1965).
47. A. Yamilov and H. Cao, *Phys. Rev. B* **68**, 085111 (2003).
48. X. Liu, W. Wu, H. Cao, and R. P. H. Chang, *J. Appl. Phys.* **95**, 3141 (2004).
49. A. Yamilov, X. Wu, and H. Cao, *J. Appl. Phys.* **98**, 103102 (2005).
50. E. W. Seelig, B. Tang, A. Yamilov, H. Cao, and R. P. H. Chang, *Mater. Chem. Phys.* **80**, 257 (2003); M. Scharrer, X. Wu, A. Yamilov, H. Cao, and R. P. H. Chang, *Appl. Phys. Lett.* **86**, 151113 (2005); M. Scharrer, A. Yamilov, X. Wu, H. Cao, and R. P. H. Chang, *ibid.* **88**, 201103 (2006).
51. A. Taflove and S. C. Hagness, *Computational Electrodynamics* (Artech House, Boston, 2000), 2nd ed.
52. T. S. Misirpashaev and C. W. J. Beenakker, *Phys. Rev. A* **57**, 2041 (1998); A. L. Burin, M. A. Ratner, H. Cao, and R. P. H. Chang, *Phys. Rev. Lett.* **87**, 215503 (2001).
53. J. P. Dowling, M. Scalora, M. J. Bloemer, and C. M. Bowden, *J. Appl. Phys.* **75**, 1896 (1994); V. I. Kopp, B. Fan, H. K. M. Vithana, and A. Z. Genack, *Opt. Lett.* **23**, 1707 (1998); N. Susa, *Jpn. J. Appl. Phys.* **40**, 142 (2001).
54. K. Sakoda, K. Ohtaka, and T. Ueta, *Opt. Express* **4**, 481 (1999).
55. H. Y. Ryu, S. H. Kwon, Y. J. Lee, Y. H. Lee, and J. S. Kim, *Appl. Phys. Lett.* **80**, 3476 (2002).
56. A. L. Burin, M. A. Ratner, H. Cao, and S. H. Chang, *Phys. Rev. Lett.* **88**, 093904 (2002).
57. R. C. McPhedran, L. C. Botten, A. A. Asatryan, C. Martijn de Sterke, N. A. Nicorovici, and P. A. Robinson, *Aust. J. Phys.* **52**, 791 (1999).
58. A. A. Asatryan, P. A. Robinson, L. C. Botten, R. C. McPhedran, N. A. Nicorovici, and C. Martijn de Sterke, *Phys. Rev. E* **62**, 5711 (2000).
59. P. L. Gourley, J. R. Wendt, G. A. Vawter, T. M. Brennan, and B. E. Hammons, *Appl. Phys. Lett.* **64**, 687 (1994); R. D. Meade, A. Devenyi, J. D. Joannopoulos, O. L. Alerhand, D. A. Smith, and K. Kash, *J. Appl. Phys.* **75**, 4753 (1994); T. F. Krauss, R. M. de la Rue, and S. Brand, *Nature* **383**, 699 (1996).
60. S. G. Johnson, S. Fan, P. R. Villeneuve, J. D. Joannopoulos, and L. A. Kolodzeski, *Phys. Rev. B* **60**, 5751 (1999).
61. E. Chow, S. Y. Lin, S. G. Johnson, P.R. Villeneuve, J:D.Joannopoulos, J.R. Wendt, G.A. Vawter, W. Zubrzycki, H. Hou, and A. Alleman, *Nature* **407**, 983 (2000).
62. O. J. Painter, R. K. Lee, A. Scherer, A. Yariv, J. D. O'Brien, P. D. Dapkus, and I. Kim, *Science* **284**, 1819 (1999).
63. S. Noda, A. Chutinan, and M. Imada, *Nature* **407**, 608 (2000).
64. M. Lončar, T. Yoshie, A. Scherer, P. Gogna, and Y. Qiu, *Appl. Phys. Lett.* **81**, 2680 (2002).
65. Y. Akahane, T. Asano, B. S. Song, and S. Noda, *Nature* **425**, 944 (2003).
66. H. G. Park, S. H. Kim, S. H. Kwon, Y. G. Ju, J. K. Yang, J. H. Baek, S. B. Kim, and Y. H. Lee, *Science* **305**, 1444 (2004).
67. B. S. Song, S. Noda, T. Asano, and Y. Akahane, *Nat. Mater.* **4**, 207 (2005).

78. S. Nojima, Jap. J. Appl. Phys. **37** (Part 2), L565 (1998).
79. M. Meier, A. Mekis, A. Dodabalapur, A. Timko, R. E. Slusher, J. D. Joannopoulos, and O. Nalamasu, Appl. Phys. Lett. **74**, 7 (1999); M. Notomi, H. Suzuki, and T. Tamamura, *ibid.* **78**, 1325 (2001); S. Noda, M. Yokoyama, M. Imada, A. Chutinan, and M. Mochizuki, Science **293**, 1123 (2001).
80. M. Imada, S. Noda, A. Chutinan, T. Tokuda, M. Murata, and G. Sasaki, Appl. Phys. Lett. **75**, 316 (1999).
81. L. Florescu, K. Busch, and S. John, J. Opt. Soc. Am. B **19**, 2215 (2002).
82. P. Villeneuve, S. Fan, S. G. Johnson, and J. D. Joannopoulos, IEE Proc.-Optoelectron. **145**, 384 (1998); E. Miyai and K. Sakoda, Opt. Lett. **26**, 740 (2001).
83. V. M. Apalkov and M. E. Raikh, Phys. Rev. Lett. **90**, 253901 (2003).
84. S. G. Johnson and J. D. Joannopoulos, Opt. Express **8**, 173 (2001).
85. C. Monat, C. Seassal, X. Letartre et al. Appl. Phys. Lett. **81**, 5102 (2002).
86. J. M. Rico-Garcia, J. M. Lopez-Alonso, and J. Alda, Opt. Express **13**, 3802 (2005).
87. O. Painter, J. Vuckovic, and A. Scherer, J. Opt. Soc. Am. B **16**, 275 (1999).
88. M. N. Shkunov, Z. V. Vardeny, M. C. DeLong, R. C. Polson, A. A. Zakhidov, and R. P. Baughman, Adv. Funct. Mater. **12**, 21 (2002).
89. B. Payne, A. Yamilov, and S. E. Skipetrov, Phys. Rev. B **82**, 024205 (2010); B. Payne, J. Andreasen, H. Cao, and A. Yamilov, *ibid.* **82**, 104204 (2010); B. Payne, H. Cao, and A. Yamilov, Physica B **405**, 3012 (2010); A. Yamilov and B. Payne, J. Mod. Opt. **57**, 1916 (2010).
90. A. N. Poddubny and E. L. Ivchenko, Physica E **42**, 1871 (2010).
91. J.-K. Yang, S. V. Boriskina, H. Noh, M. J. Rooks, G. Solomon, L. Dal Negro, and H. Cao, Appl. Phys. Lett. **97**, 223101 (2010).

